

Tetrahedral Mesh Improvement by Shell Transformation

Jianjun Chen^{a*}, Jianjing Zheng^a, Yao Zheng^a, Zhoufang Xiao^a, Hang Si^b, Yufeng Yao^c

^a Center for Engineering and Scientific Computation, and School of Aeronautics and Astronautics, Zhejiang University, Hangzhou 310027, China

^b Weierstrass Institute for Applied Analysis and Stochastics, Mohrenstrasse 39, 10117 Berlin, Germany

^c Faculty of Environment and Technology, University of the West of England, Bristol BS16 1QY, United Kingdom

ABSTRACT

Existing flips for tetrahedral meshes simply make a selection from a few possible configurations within a single shell (i.e., a polyhedron that can be filled up with a mesh composed of a set of elements that meet each other at one edge), and their effectiveness is usually confined. A new topological operation for tetrahedral meshes named *shell transformation* is proposed. Its recursive callings execute a sequence of shell transformations on neighboring shells, acting like *composite edge removal* transformations. Such topological transformations are able to perform on a much larger element set than that of a single flip, thereby leading the way towards a better local optimum solution. Hence, a new mesh improvement algorithm is developed by combining this recursive scheme with other schemes, including smoothing, point insertion and point suppression. Numerical experiments reveal that the proposed algorithm can well balance some stringent and yet sometimes even conflict requirements of mesh improvement, i.e., resulting in high-quality meshes and reducing computing time at the same time. Therefore, it can be used for mesh quality improvement tasks involving millions of elements, in which it is essential not only to generate high-quality meshes, but also to reduce total computational time for mesh improvement.

KEY WORDS: mesh improvement; mesh generation; shell transformation; mesh smoothing; topological transformation; tetrahedral meshes

1. INTRODUCTION

For numerical simulations with complex geometries, mesh generation typically represents a large portion of the overall computational time. Thus, the ability of performing computations on large-scale tetrahedral elements has always been regarded as an important issue. The fundamental reason is mainly because a theoretically valid tetrahedral mesh can always be automatically generated for a valid 3D domain [1-5], despite that this is not always the case for other specific types of volume elements. Despite of the validity, the quality of an initial tetrahedral mesh produced by a mesher may not be high enough for simulations. A follow-up mesh improvement step is thus indispensable to remove those poorly shaped elements contained in the initial meshes to prevent their adverse effects on the stability and accuracy of the simulations.

In general, a mesh improver executes the following types of local operations iteratively:

- (1) *Smoothing*, which repositions mesh points to improve the quality of adjacent elements.
- (2) *Local reconnection*, which replaces a local mesh with another mesh that fills up the same region. The new mesh will have the same point set as the old mesh but applying different point connections.

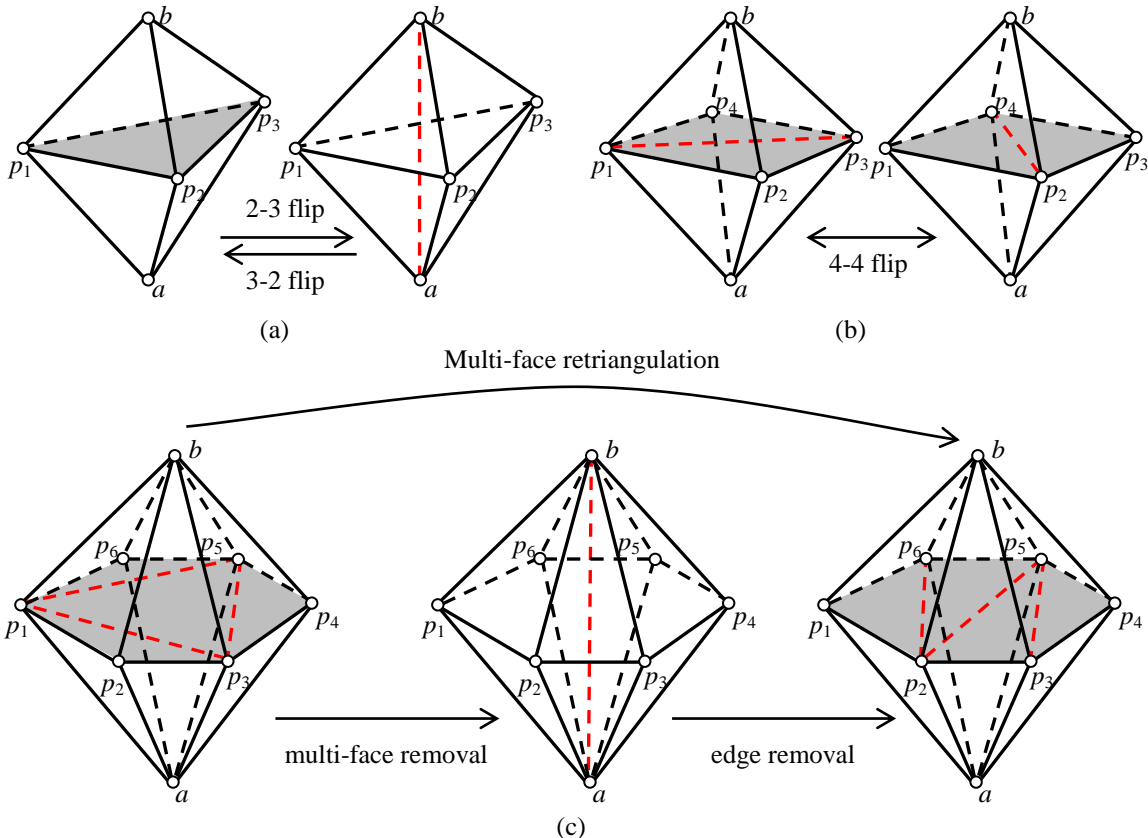
* Corresponding author. E-mail: chenjj@zju.edu.cn

41 (3) *Point insertion/suppression*, which improves a mesh by inserting new points into the
 42 mesh or removing existing points from the mesh.

43 Our primary focus in this study is on local reconnection, although all the local operations
 44 mentioned above will be combined in the developed mesh improver. If the point set is fixed,
 45 the quality of mesh elements is apparently determined by how these points are connected. It is
 46 unrealistic to search for a global optimal mesh topology by directly iterating a large number of
 47 possible solutions to connect a point set because this number could expand exponentially with
 48 the increase of the number of points. Thus, heuristics prevail in improving the quality of a
 49 mesh by iteratively changing the local connections of points.

50 The most frequently used local reconnection technique for tetrahedral meshes is based on
 51 *elementary flips* [6], including 2-3, 3-2 and 4-4 flips (note that the numbers in these names
 52 denote the number of tetrahedra removed and created by the flips, respectively; see Figures 1a
 53 and 1b). Because the elementary flips simply make a selection from several possible
 54 configurations within a relatively small region, their effectiveness in mesh quality
 55 improvement is usually confined. To overcome this limit, three advanced flips that involve
 56 more elements were later suggested, i.e., *edge removal* [7], *multi-face removal* [8] and *multi-*
 57 *face retriangulation* [9] (see Figure 1c). They enrich the possible configurations within
 58 relatively larger regions and therefore behave more effectively in mesh quality improvement
 59 than the elementary flips.

60
61



62
63

64 **Figure 1.** Existing flips for a tetrahedral mesh: (a) 2-3 flip and 3-2 flip; (b) 4-4 flip; (c) multi-
 65 face removal, edge removal and multi-face retriangulation.

66 In general, the effect of a local reconnection technique highly depends on the size of a local
 67 mesh it treats. The more elements it treats during one operation; the more possibility it
 68 improves the quality of a local mesh to a higher level. This motivates the development of
 69 more aggressive local reconnection techniques for mesh quality improvement. For instance,
 70 Joe [6] once proposed nine schemes to *combine the elementary flips* for mesh improvement.
 71 Later, Shewchuk [10] pointed out that the composite flips proposed by Joe [6] could be

72 expressed as one or two edge removal operations. Thus, Shewchuk suggested that the study of
73 composite edge removal transformations was a fruitful direction for mesh improvement
74 research. Unfortunately, Shewchuk did not present details about what such composite
75 transformations are and how to implement such transformations efficiently. As a result, it was
76 observed that no composite transformations are actually incorporated into the open-source
77 tetrahedral improver (namely Stellar thereafter) developed by Klinger and Shewchuk [11, 12].

78 The main contribution of this present study is the development of a new local reconnection
79 technique that could act like composite edge removal transformations. This technique is based
80 on the recursive callings of a new flip named *shell transformation*. The single calling of shell
81 transformation could be considered as an enhanced version of edge removal transformation.
82 However, an essential difference exists between two approaches, and enables shell
83 transformation to be executed recursively (see Section 2.4 for details). Thus, edge removal
84 only makes a selection from a few possible configurations within a single shell (i.e., a
85 polyhedron that can be filled up with a mesh composed of a set of elements that meet each
86 other at one common edge). However, the recursive callings of shell transformations can
87 execute a sequence of shell transformations on neighboring shells. In other words, recursive
88 shell transformations could be performed on a much larger element set than that of edge
89 removal, thereby leading the way towards a better local optimum solution.

90 Another focus of this study is about the efficient implementation of the new local
91 reconnection technique, because local reconnections need to be employed for a large number
92 of times during the entire mesh improvement workflow. The dynamic programming algorithm
93 suggested by Shewchuk for edge removal [10, 13] will be revisited at first and then further
94 enhanced to implement the basic shell transformation routine. Besides, the computing
95 efficiency of recursive callings of shell transformations is investigated carefully because the
96 number of such callings may increase exponentially when the recursive level increases.
97 Reasonable restrictions are provided to prevent inefficient recursive callings. Meanwhile,
98 several strategies are suggested to improve the efficiency.

99 Finally, the ability of the proposed local reconnection technique will be demonstrated by
100 performing various mesh improvement tasks, some of which involve millions of elements. In
101 a pipeline of producing meshes of this magnitude, mesh generation itself may only consume a
102 few seconds computing time, owing to recent advancement in the field of fast and parallel
103 mesh generation techniques [14-17]. However, a mesh improver possibly consumes many
104 minutes computing time or even longer in order to manage such a big mesh. Therefore, to
105 ensure the applicability of this newly developed mesh improver for large-scale problems, an
106 essential requirement we will take into account is the *cost-effectiveness* of the mesh improver,
107 i.e., the ability to balance the conflict requirements of resulting in a high-quality mesh and
108 saving computing time of mesh improvement. Following this concept, a set of existing
109 smoothing, point insertion and point suppression schemes are selected. Combining these
110 schemes with the proposed local reconnection technique, a cost-effective improver applicable
111 to large-scale meshes is therefore developed and verified.

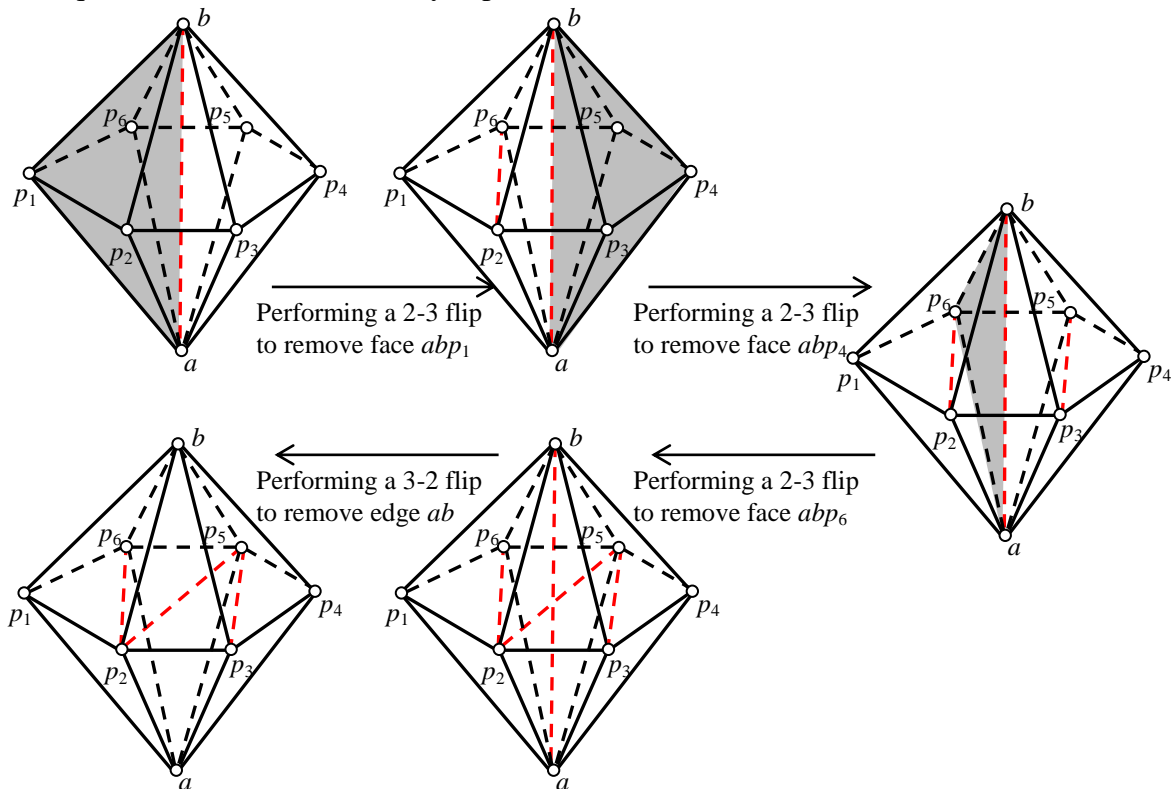
112 The remainder of this article will be organized as follows. In Section 2, related works are
113 firstly reviewed, followed by the introduction of the new local reconnection technique in
114 Section 3. Section 4 describes the basic implementation of shell transformation, while
115 Section 5 presents the recursive scheme of shell transformation and the local reconnection
116 scheme based on this recursive scheme. Section 6 introduces other local operations that are
117 combined to form the developed new mesh improver. Section 7 provides various examples of
118 numerical experiments demonstrating the effectiveness and efficiency of the proposed
119 scheme. Section 8 concludes with outcomes of the study.

2. RELATED WORKS

121 Firstly, related works on local reconnection techniques are reviewed in details (see Section
 122 2.1). After that, a brief review on other types of local operations (see Sections 2.2 and 2.3,
 123 respectively) is presented to justify our choices of these types of operations in the developed
 124 mesh improver.

125 2.1 Related work on local reconnection techniques

126 Local reconnection techniques are frequently used in various circumstances of mesh
 127 generation, such as Delaunay refinement [18], mesh adaptation [19], boundary recovery [1-5],
 128 and mesh quality improvement [6-12, 20, 21]. The first type of local reconnection techniques
 129 is based on the flips presented in Figure 1. The 3-2, 2-3 and 4-4 flips are defined as
 130 *elementary flips*, not only because they are special cases of the advanced flips, but also
 131 because they could be combined to form the advanced flips. For instance, the edge removal
 132 transformation could be implemented as a sequence of 2-3 flips followed by a single 3-2 flip
 133 (see Figure 2) [10]. This possibly explains why Shewchuk [10] judged that the composite
 134 transformations of the elementary flips proposed earlier by Joe [6] could be expressed as one
 135 or two edge removal transformations. However, this does not mean that a local reconnection
 136 technique based on the elementary flips could achieve the same effect as the techniques based
 137 on the advanced flips. In general, the advanced flips provide elaborate ‘*patterns*’ for how to
 138 combine the elementary flips such that those involved elementary flips could work together in
 139 a much larger element set. As a result, the local reconnection techniques based on the
 140 advanced flips could usually improve the quality of a mesh to a higher level than that by the
 141 techniques based on the elementary flips.



142
 143

144 **Figure 2.** Implementing edge removal as a sequence of 2-3 flips followed by a 3-2 flip.

145 Differently, Liu *et al.* proposed to improve mesh quality by a local remeshing technique
 146 named *small polyhedron reconnection* (SPR) [21]. The SPR algorithm initializes an empty

147 polyhedron in the neighbourhood of a poorly shaped element, and then performs an
148 exhaustive search to find the *optimal* tetrahedralization of this polyhedron. Typically, the
149 advanced flips treat only a local mesh composed of a few tetrahedral elements, while the SPR
150 algorithm can search for the optimal tetrahedralization of a polyhedron composed of 20-40
151 tetrahedral elements. Consequently, it was reported that the SPR algorithm could achieve a
152 better mesh improvement result than that of the flip-based algorithm [21]. However, the main
153 issue of the SPR algorithm is its computing complexity, since the problem of meshing an
154 empty polyhedron is NP hard. Although some strategies have been proposed in the past to
155 improve the timing-related performance of the SPR algorithm [4, 21], our experience shows
156 that, if the local reconnection scheme of a mesh improver is completely dependent on the SPR
157 algorithm. In addition, the runtime of a mesh improver may be beyond the user's expectation,
158 in particular when the treated mesh is composed of one million or more elements.

159 2.2 Related work on mesh smoothing

160 The mesh smoothing methods can be classified into two categories in general, i.e., the
161 Laplacian-type method [22] and the optimization-based method [20, 23-28]. The Laplacian-
162 type method moves each mesh vertex towards the *center* of its neighboring vertices. It
163 provides no guarantee for the improvement of mesh quality, therefore leading to either low
164 quality or even possibly invalid elements. To overcome this drawback, various optimization-
165 based approaches were proposed. These approaches can be divided into two types in
166 accordance with the choice of objective functions. The *local* method maximizes a quality
167 function for the elements surrounding each mesh vertex by relocating mesh vertices
168 iteratively [20, 23, 24]. The *global* method maximizes a quality function for all elements by
169 relocating all mesh vertices simultaneously [25-28]. While the local method may improve an
170 element at a cost of degrading its neighboring elements, the global method relieves this
171 conflict to some extents by considering the quality of the entire mesh as a whole.
172 Nevertheless, because the global method needs to solve a large-scale optimization model, the
173 choice of solution methods for this optimization model will be the key step to achieve
174 acceptable computing time and performance [28]. Likewise, in the case of surface mesh
175 smoothing, various *local* and/or *global* shape-preserving approaches have been developed, in
176 which the global approach based on geometric flows is now still prevailing because of its
177 powerful ability to preserve geometric features and thus reduce volume shrinkage [25].

178 Since the cost-effectiveness of a new mesh improver is our primary goal to achieve, we
179 select a local approach instead of a more time-consuming global approach for mesh
180 smoothing. More specifically, we combine an optimization-based algorithm [20] with the
181 Laplacian smoothing [22]. See Section 5.4 later for more details.

182 2.3 Related work on point insertion and point suppression

183 It is intuitive to eliminate low-quality elements by inserting vertices into existing meshes.
184 Typically, a new vertex can be located at the circumcenter [5, 29] or centroid of a poor
185 element [1, 4], or the midpoint of the longest edge of this element [2, 30]. One typical strategy
186 to insert this kind of vertex into a mesh is by Delaunay refinement [1-5, 29, 31], or more
187 simply, by splitting the element(s) containing the new vertex (which may result in temporary
188 low-quality elements) firstly and then improving the mesh by combining smoothing and local
189 reconnection [19]. Besides, Klingner and Shewchuk suggested an effective but very time-
190 consuming point insertion scheme that combines a Delaunay-type algorithm with smoothing
191 operations [11]. It is possible that hundreds of elements are involved in just one single
192 operation. Nevertheless, to meet our goal of developing a cost-effective mesh improver for
193 large-scale problem inputs, we adopt an *edge-splitting* based point insertion scheme.

194 As a reverse operation of point insertion, it is not surprising that point suppression can also
 195 improve local mesh quality by remeshing an empty polyhedron composed of all elements
 196 surrounding the vertex to be removed. The challenge mainly comes from those polyhedra that
 197 cannot be tetrahedralized if no Steiner points are allowed [31]. Meanwhile, even if a
 198 polyhedron can be tetrahedralized without inserting Steiner points (although the prediction of
 199 this is NP hard [31]), it is not easy to find an optimal mesh to fill in that polyhedron (it is also
 200 NP hard [4, 21]). Theoretically, the SPR algorithm mentioned in Section 2.1 [4, 21] could be
 201 a good candidate for remeshing an empty polyhedron because it can provide an optimal
 202 solution when the polyhedron is meshable. Nevertheless, as we pointed earlier, the main issue
 203 of the SPR algorithm is its relatively poor timing performance. Therefore, we adopt an *edge-*
 204 *contraction* based point suppression routine that is available from Stellar [12, 13].

205 See Section 5.5 later for the developed point insertion and suppression schemes.

206 3. SHELL TRANSFORMATION AND ITS RECURSIVE CALLINGS: 207 THE MAIN IDEA

208 For the completeness, we have briefly reviewed different types of local operations in order to
 209 justify our choices. However, it must be emphasized that the main contribution of this study is
 210 the development of a new local reconnection technique. With respect to other local
 211 operations, we only select a suitable operation among various existing approaches to meet our
 212 goal of developing a cost-effective mesh improver.

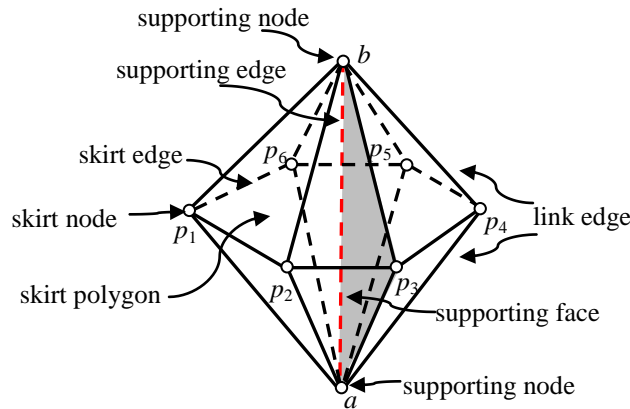
213 Before introducing the new local reconnection technique, Figure 3 illustrates some
 214 terminologies in relation with a shell structure because all of the flips discussed in this study,
 215 including those presented earlier in Figure 1 and the new proposed shell transformation, will
 216 involve this structure.

217 It was reported that edge removal might be the most effective flip for mesh quality
 218 improvement [12], although other flips could provide marginal improvements additionally. To
 219 remove a low-quality element (for instance, the element abp_5p_6 in Figure 4), we could pick up
 220 an edge of this element (denoted by e), and perform the edge removal transformation in the
 221 shell of e (i.e., e is the supporting edge of the shell). For instance, e refers to ab in Figure 4. If
 222 the output covering mesh of the transformation is better than the old one, edge removal
 223 succeeds and the low-quality element is removed (since e is removed). In such a case, the
 224 skirt polygon of the shell is *completely triangulated* (see Figure 4). However, it is not
 225 uncommon that the edge removal could not provide a better mesh than the old one and thus
 226 fails to remove e and the low-quality element bounded by e . Instead, a covering mesh of the
 227 shell that is better than the old one might be the one shown in the bottom of Figure 4, where a
 228 *core* referring to the unmeshed part of the skirt polygon exists in the resulting mesh. In this
 229 case, we say the shell of e can only be partially reduced[†], and the remaining supporting faces
 230 must be removed to reduce the shell further. Obviously, if one of the link edges that bound a
 231 supporting face f is removed, f will be removed accordingly. For the case shown in the bottom
 232 of Figure 4, f could be the face abp_5 , and the link edge could be ap_5 or bp_5 . Assuming that ap_5
 233 is picked up for removal, the above transformation is called again to reduce the shell of ap_5 . If
 234 the reduced shell of ap_5 does not contain the face abp_5 and any new supporting faces sharing

[†]Here, the *degree* of a covering mesh refers to the number of elements that share the supporting edge in this mesh. A shell is *reduced* if the degree of the new covering mesh is becoming smaller than that of the old mesh. In particular, if the degree of the new mesh becomes zero, the shell is *completely reduced*, and the new mesh is a *completely reduced mesh*; otherwise, the shell is *partially reduced*, and the new mesh is a *partially reduced mesh*.

235 ab , the shell of ab is reduced as well; otherwise, a process that attempts to remove the
 236 supporting faces around ap_5 is repeated.

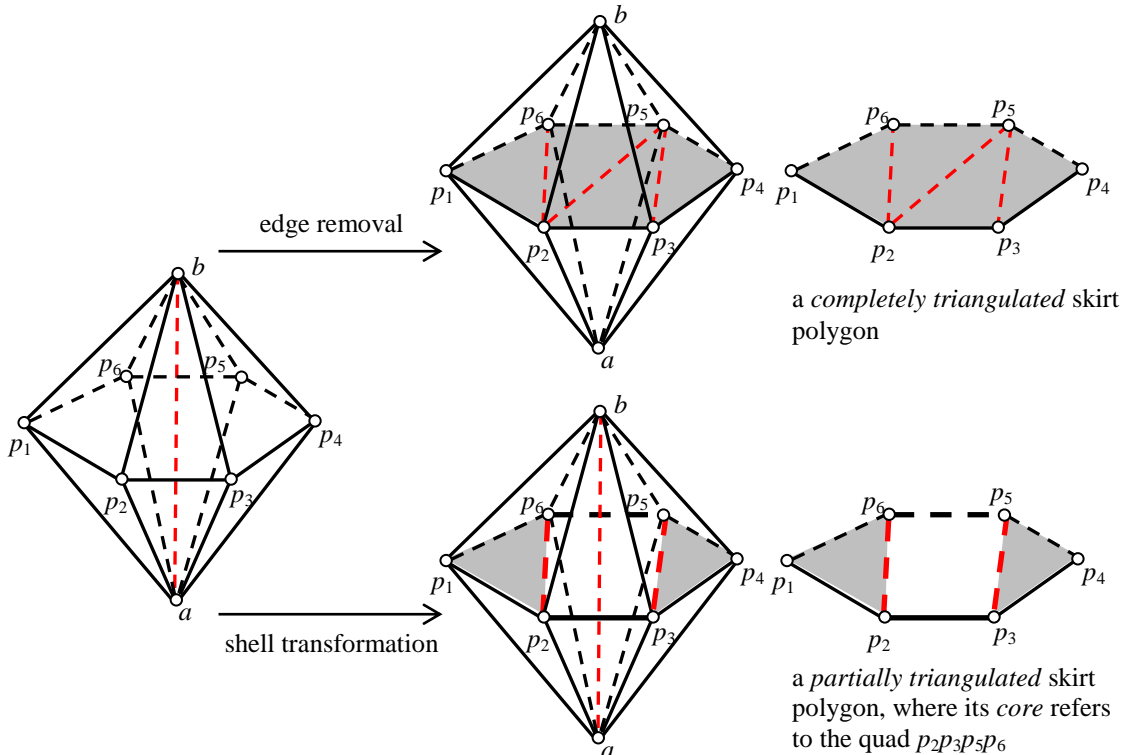
237 To better understand the above recursive scheme, Figure 5 illustrates how this scheme
 238 works on a local mesh composed of two shells (see Figure 5a), aimed at removing the edge ab
 239 from the mesh. Firstly, a transformation is called on the shell of ab . Since the shell cannot be
 240 completely reduced, the edge ab still exists in the output mesh (see Figure 5b). Nevertheless,
 241 the degree of the shell is reduced from 5 to 4. To reduce the shell further, a link edge bh is
 242 picked up and a transformation is called on the shell of bh and reduces this shell completely.
 243 Besides, the degree of the shell of ab is reduced from 4 to 3 after this step (see Figure 5c).
 244 Finally, a transformation is called to update the shell of ab to remove ab by a single 3-2 flip
 245 (see Figure 5d for the final output).



246

247

Figure 3. The terms defined for the mesh entities of a shell.

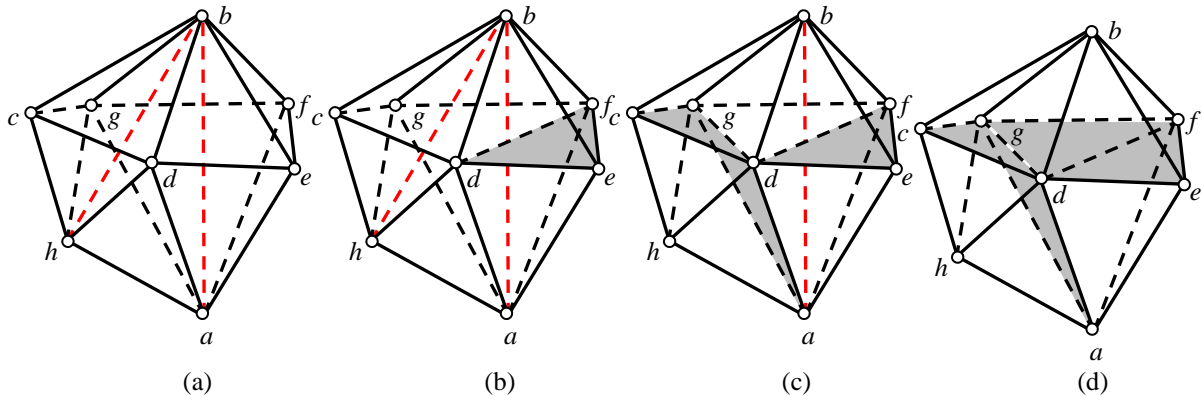


248

249 **Figure 4.** The difference between edge removal and a single calling of shell transformation.
 250 This difference enables shell transformation to be called recursively while edge removal
 251 cannot. This recursive ability is the main advantage of shell transformation technique.

252 Here, given the covering mesh of a shell, the transformation that attempts to reduce the

253 shell is denoted as *shell transformation*. The main *difference* between shell transformation
 254 and edge removal is that shell transformation allows the output mesh containing a *partially*
 255 *triangulated* skirt polygon while edge removal does not. If the output covering mesh of shell
 256 transformation does not contain a *core*, shell transformation is the same operation as edge
 257 removal. In this respect, edge removal could be considered a special case of shell
 258 transformation. In other words, shell transformation could be considered as an enhanced
 259 version of edge removal because it considers more possibility to mesh a shell. Moreover, *the*
 260 *main advantage of shell transformations is rooted in its recursive ability*. As Joe have
 261 demonstrated [6] that the composite transformations of elementary flips could improve the
 262 quality of a mesh to a much higher level than elementary flips, and the recursive callings of
 263 shell transformations, acting like composite edge removal transformations, could perform
 264 much better than edge removal in most mesh improvement tasks, as we will demonstrate in
 265 Section 6.



268 **Figure 5.** Illustration for the recursive callings of shell transformations. (a) The input mesh.
 269 (b) The output after the first shell transformation calling on the shell of ab . (c) The output
 270 after the second shell transformation calling on the shell of bh . (d) The final output after the
 271 third shell transformation calling on the shell of ab .

272 4. A SINGLE CALLING OF SHELL TRANSFORMATION

273 To implement a shell transformation procedure, a key step is to develop an algorithm that can
 274 triangulate a skirt polygon *partially*. Meanwhile, among all of the valid triangulation schemes,
 275 an algorithm needs to find the triangulation corresponding to an *optimal* covering mesh. In
 276 this section, we will first reproduce a dynamic programming algorithm suggested by
 277 Shewchuk [10], which can be used to triangulate the skirt polygon *completely* and optimally.
 278 Next, the proposed shell transformation algorithm is described in details, which enhances the
 279 Shewchuk's algorithm in order to triangulate the skirt polygon *partially* and optimally.

280 4.1 The algorithm proposed by Shewchuk [10]

281 Given a shell covered by a set of tetrahedra $p_i p_{i+1} ab (i=1, 2, \dots, m)$, each triangulation
 282 $T = \{t_1, t_2, \dots, t_{m-2}\}$ of the skirt polygon induces a tetrahedralization of the shell:

$$283 \quad K = \{\text{conv}(t_i, a) \cup \text{conv}(t_i, b) \mid i=1, 2, \dots, m-2\}.$$

284 Here, $\text{conv}(\cdot)$ refers to a tetrahedron formed by a face and a node. We define the quality of
 285 T to be the quality of the worst tetrahedron within the tetrahedralization K .

286 For each node $p_i (1 \leq i \leq m)$, p_{i+m} is its alias. $R_{i,j}$ defines a ring of edges whose ending
 287 nodes are

$$P_{i,j} = \begin{cases} \{p_i, p_{i+1}, \dots, p_j\} & 1 \leq i < j \leq m \\ \{p_j, p_{j+1}, \dots, p_{i+m}\} & 1 \leq j < i \leq m \end{cases}.$$

Selecting a node $p_k \in P_{i,j}$ other than p_i and p_j , the triangulation of $R_{i,j}$ includes three parts, as shown in Figure 6:

$$T_{i,j} = T_{i,k} \cup T_{k,j} \cup \Delta p_i p_k p_j.$$

We can define a matrix M_q to record the quality of the optimal triangulation of $R_{i,j}$ as:

$$M_q(i, j) = \max_{p_k \in P_{i,j}, p_k \neq p_i, p_j} \min\{M_q(i, k), M_q(k, j), q(a, p_i, p_j, p_k), q(p_i, p_j, p_k, b)\}, \quad (1)$$

where $q(\cdot)$ is the quality function for tetrahedral elements. $M_q(i, j) = \infty$ when $j = i + 1$. Since $1 \leq i, j \leq m$ (m refers to the size of the skirt polygon), we know M_q is a $m \times m$ matrix.

Based on Equation 1, Algorithm 1 fills in the upper triangular part of M_q by an order of decreasing i and increasing j so that $M_q(i, k)$ and $M_q(k, j)$ are computed before $M_q(i, j)$. Meanwhile, Algorithm 1 fills in another matrix M_k that records the values of k that maximize Equation 1 in order to reconstruct the optimal triangulation T^{opt} :

$$\begin{cases} T^{\text{opt}} = T_{1,m}^{\text{opt}} \\ T_{i,j}^{\text{opt}} = T_{i,k}^{\text{opt}} \cup T_{k,j}^{\text{opt}} \cup \Delta p_i p_k p_j \quad (k = M_k(i, j)) \end{cases}.$$

Algorithm 1. Filling in the upper triangular part of M_q and M_k

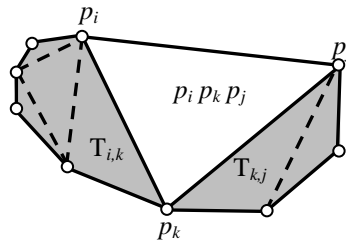
fillInMatrices_UpRight(a, b, P, M_q, M_k)

Inputs:

a and b : the support nodes of a shell,

$P = \{p_1, p_2, \dots, p_m\}$: the skirt polygon of a shell

1. **for** $i = m - 2$ **downto** 1
 2. **for** $j = i + 2$ **to** m
 3. **for** $k = i + 1$ **to** $j - 1$
 4. $q = \min\{q(a, p_i, p_k, p_j), q(p_i, p_k, p_j, b)\}$
 5. **if** $k < j - 1$
 6. $q = \min\{q, M_q(k, j)\}$
 7. **if** $k > i + 1$
 8. $q = \min\{q, M_q(i, k)\}$
 9. **if** $k = i + 1$ **or** $q > M_q(i, j)$
 10. $M_q(i, j) = q$
 11. $M_k(i, j) = k$
-



$$T_{i,j} = T_{i,k} \cup T_{k,j} \cup \Delta p_i p_k p_j$$

Figure 6. Decomposing a triangulation optimization problem into sub-problems.

306 4.2 The proposed shell transformation algorithm

307 Firstly, we introduce the concept of *triangulation graph*. It is a directed graph defined on a
 308 polygon that is bounded by a set of nodes $P = \{p_1, p_2, \dots, p_m\}$. A *graph node* corresponds to a
 309 polygon node, and a graph edge $\langle p_i, p_j \rangle$ exists if there are valid triangulations for the ring
 310 $R_{i,j}$. Note that \mathbf{M}_q provides a representation of the triangulation graph: $\mathbf{M}_q(i, j) > 0$
 311 means that there is a valid triangulation for the ring $R_{i,j}$; thus, $\langle p_i, p_j \rangle$ is a graph edge.

312 Algorithm 1 only fills in one half of \mathbf{M}_q and \mathbf{M}_k . To get a complete representation of
 313 the triangulation graph, the lower left elements of \mathbf{M}_q and \mathbf{M}_k must be computed.
 314 Algorithm 2 present a routine that fills in all of useful elements of \mathbf{M}_q and \mathbf{M}_k , which
 315 could be located in either side of the main diagonal of the two matrices. In the new algorithm,
 316 one diagonal of \mathbf{M}_q and \mathbf{M}_k is computed at a time in the increasing order of the size of
 317 $R_{i,j}$ (i.e., number of vertices). Note that after calling Algorithm 2, $\mathbf{M}_q(1, m)$, and
 318 $\mathbf{M}_q(2, 1), \dots$, and $\mathbf{M}_q(m, m-1)$ all records the quality of the optimal triangulation of the
 319 complete skirt polygon, but with different start and end vertices. Based on Algorithm 2, we
 320 could then implement a single calling of shell transformation (see Algorithm 3), where a key
 321 step is to define the *core* of the shell. As shown in Figure 7, the core introduced in shell
 322 transformation corresponds to a simple cycle of the triangulation graph of the skirt polygon.
 323 Therefore, once the graph is set up by calling Algorithms 1 and 2, all of the simple cycles are
 324 visited, and the optimal one is picked up to reconstruct the triangulation of the skirt polygon
 325 (i.e., Line 5 of Algorithm 3). Here, a simple cycle is identified as optimal when it corresponds
 326 to an optimal covering mesh (K). Note that the definition on the optimality of a mesh could be
 327 application specific, see Section 4.3 for details.

328 **Algorithm 2.** Filling in \mathbf{M}_q and \mathbf{M}_k

fillInMatrices($a, b, P, \mathbf{M}_q, \mathbf{M}_k$)

Inputs:

a and b : the support nodes of a shell

$P = \{p_1, p_2, \dots, p_m\}$: the skirt polygon of a shell

1. **for** $d = 2$ **to** $m - 1$
 2. **for** $i = 1$ **to** m
 3. $j' = i + d$
 4. **for** $k' = i + 1$ **to** $j' - 1$
 5. $j = j' > m ? j' - m : j'$
 6. $k = k' > m ? k' - m : k'$
 7. $q = \min\{q(a, p_i, p_k, p_j), q(p_i, p_k, p_j, b)\}$
 8. **if** $k' < j' - 1$
 9. $q = \min\{q, \mathbf{M}_q(k, j)\}$
 10. **if** $k' > i + 1$
 11. $q = \min\{q, \mathbf{M}_q(i, k)\}$
 12. **if** $k' = i + 1$ **or** $q > \mathbf{M}_q(i, j)$
 13. $\mathbf{M}_q(i, j) = q$
 14. $\mathbf{M}_k(i, j) = k$
-

329 Assuming that the node set of the core is $P_c = \{p_{c_1}, \dots, p_{c_n}, p_{c_{n+1}} = p_{c_1}\}$, the reconstructed
 330 triangulation is (see Figure 7):
 331

$$332 \quad T^{\text{opt}} = \{T_{c_j, c_{j+1}}^{\text{opt}} \mid j = 1, 2, \dots, n\}$$

333 The new covering mesh of the shell is:

$$K = K_1 \cup K_2$$

$$334 \quad K_1 = \{\text{conv}(t_i, a) \cup \text{conv}(t_i, b) \mid t_i \in T^{\text{opt}}\}, \quad (2)$$

$$K_2 = \{\text{tetr}(p_{c_j}, p_{c_{j+1}}, a, b) \mid j = 1, 2, \dots, n\}$$

335 where $\text{tetr}(\cdot)$ refers to the tetrahedral element formed by four specified nodes.

336 **Algorithm 3.** A general routine of shell transformation

shellTransformation(a, b, P, K_{old})

Inputs:

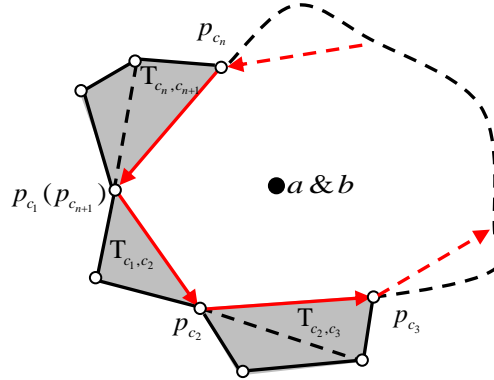
a and b : the support nodes of the shell

$P = \{p_1, p_2, \dots, p_m\}$: the skirt polygon of the shell

K_{old} : the old covering mesh of the shell

1. **fillInMatrices_UpRight**(a, b, P, M_q, M_k)
 2. **fillInMatrices_LowLeft**(a, b, P, M_q, M_k)
 3. G : the triangulation graph with M_q as its matrix representation
 4. P_c : an *optimal* simple cycle of G
 5. T^{opt} : the reconstructed triangulation from P_c , see Figure 6
 6. K : the new covering mesh of the shell, see Equation 2
 7. **if** $K \neq \emptyset$ **and** $K \neq K_{\text{old}}$
 8. Remesh the shell by replacing K_{old} with K
-

337



338

339 **Figure 7.** Illustration for the triangulation graph of a polygon, where those lines with arrows
 340 are a group of graph edges, forming a simple cycle and thus defining a scheme that
 341 triangulates the polygon *partially*.

342 5. RECURSIVE CALLINGS OF SHELL TRANSFORMATIONS

343 5.1 The basic routine

344 A single shell transformation calling only involves a small number of elements. It may not be
 345 able to reduce a shell completely because of the constraints on the shell boundaries. Hence,
 346 we develop a routine that calls shell transformations recursively to remove these constraints.

347 Algorithm 4 details the routine of recursive shell transformations. Given an edge e , the
 348 calling **recursiveST**($e, \emptyset, 0, l_{\text{max}}$) attempts to remove the edge e , where l_{max} limits the

349 maximally allowed recursive level. Given a face f and one of its boundary edges e , the calling
 350 **recursiveST**($e, f, 0, l_{\max}$) attempts to remove the face f .

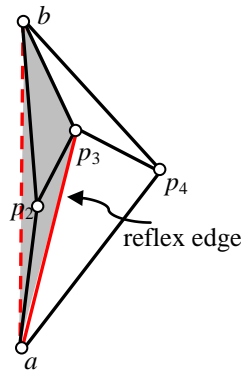
351 Note that Algorithm 4 expands an *edge tree*, where the input edge e is the *root* of this tree,
 352 and those link edges (e') inputted for further recursions are *children* of the edge e . In this
 353 manner, the tree can be expanded recursively. If a tree node v_1 is an *ancestor* of another tree
 354 node v_2 , we say the edge corresponding to v_1 is an *ancestor edge* of the edge corresponding to
 355 v_2 .

356 5.2 Termination and efficiency

357 Two routines called by Lines 10 and 3 account for the timing-related performance of
 358 Algorithm 4, namely **pickRecursiveLinkEdge** and **shellTransformation**. They determine
 359 how many shell transformations are executed and how fast a single shell transformation can
 360 run, respectively.

361 Given a supporting face f in the shell of e , the routine **pickRecursiveLinkEdge** checks
 362 whether or not a further recursion is necessary. If yes, the routine returns a link edge between
 363 two possible candidates. To filter inefficient recursions, the implementation of this routine can
 364 be further improved through the following guidelines:

- 365 (1) Do not return a boundary edge.
- 366 (2) If a tetrahedra sharing f overlaps with the shells of an ancestor edge of e , return
 367 nothing.
- 368 (3) Return a *reflex edge* only. In Figure 8, two faces ap_2p_3 and ap_3p_4 form a *reflex angle* if
 369 viewed from a point b ; correspondingly, ap_3 is called a *reflex edge* of the face abp_3 .



370 **Figure 8.** Illustrative case of a *reflex edge*.
 371

372 The termination of Algorithm 4 remains an issue because there is no guarantee that a mesh
 373 edge could be removed by flips under the requirement that the quality of the mesh could not
 374 be decreased by these flips. Although the second guideline mentioned above prevents an
 375 infinite execution of the recursive callings, Algorithm 4 could still be very time-consuming
 376 because the number of its shell transformation callings may increase exponentially when the
 377 recursive level increases. Therefore, a user parameter l_{\max} is input to Algorithm 4 to limit the
 378 maximal recursive level. Based on an analysis of many trial and error experimental results, we
 379 choose l_{\max} to be 5 in this study to meet our goal of developing a cost-effective mesh
 380 improver.

381 The routine **shellTransformation** (see Algorithm 3) includes two main steps. Firstly, it
 382 employs Algorithms 1 and 2 to obtain the triangulation graph of the skirt polygon. Next, it
 383 searches for a simple cycle in that graph to reconstruct an optimal covering mesh according to
 384 Equation 2. The time consumptions of both steps are at an order of $O(m^3)$, where m is the
 385 number of skirt nodes. A single calling of this routine may consume little time because m is
 386 very small. However, the number of callings could be very large because of the recursive
 387 nature of Algorithm 4. In our implementation, this routine has been speeded up through three
 388 treatments as follows:

- 389 (1) Introduce the validity conditions (see Section 4.3) in the first step to simplify the
390 triangulation graph;
391 (2) Search for the *optimal* simple cycle first to prevent those unnecessary searches for low-
392 quality cycles;
393 (3) Record the results of time-consuming mesh validity and quality computations after
394 they are executed for the first time so that simple queries can replace the repeated
395 callings of these computations.

396 **Algorithm 4.** The routine of recursive shell transformations

recursiveST(e, f, l, l_{\max})

Inputs:

- the supporting edge, denoted e
- a face containing e that the routine attempts to remove, denoted f
- the recursive level with an initial value of zero, denoted l
- the maximally allowed recursive level, denoted l_{\max}

Variables:

- the ending nodes of an edge, denoted $a(\cdot)$ and $b(\cdot)$
- the skirt polygon of the shell of an edge, denoted $P(\cdot)$
- the set of elements containing an edge, denoted $S(\cdot)$
- a set of link faces contained in $S(\cdot)$, denoted $F(\cdot) = \{f_1', f_2', \dots, f_m'\}$, where $m = |F(\cdot)|$

1. **if** $|S(e)| \leq 0$ **or** ($f \neq \emptyset$ **and** $f \notin F(S(e))$)
 2. **return** success
 3. **shellTransformation**($a(e), b(e), P(e), S(e)$)
 4. **if** $|S(e)| \leq 0$ **or** ($f \neq \emptyset$ **and** $f \notin F(S(e))$)
 5. **return** success
 6. **if** $l \geq l_{\max}$ /* the recursive level is limited under l_{\max} . */
 7. **return** fail
 8. $m = |S(e)|$ /* record the size of the shell $S(e)$ */
 9. **for** $i = 1$ **to** m
 10. $e' = \text{pickRecursiveLinkEdge}(f_i')$ /* filters are set to avoid inefficient recursions */
 11. **if** $e' \neq \emptyset$
 12. **recursiveST**($e', f_i', l+1, l_{\max}$) /* recursive calling */
 13. **if** $|S(e)| < m$ /* $S(e)$ is reduced as well */
 14. retrun **recursiveST**(e, f, l, l_{\max}) /* recursive calling */
 15. **return** fail
-

397 Another factor that affects the efficiency of Algorithm 4 is the routine that identifies a shell
398 in the input mesh (referring to the *shell-find* routine thereafter), which is employed by Lines 4
399 and 13 of Algorithm 4. The efficiency of this routine depends on the data structure adopted to
400 represent a tetrahedral mesh. In our scheme, four incident vertices are stored for each
401 tetrahedron, plus four neighboring elements of this tetrahedron. Meanwhile, for each mesh
402 vertex, one element incident to this vertex is stored. This data structure requires a small
403 amount of memories, and the *shell-find* routine based on it only needs to traverse the elements
404 locally. Given two ending vertices of an edge (denoted by v_1 and v_2 , respectively), the *shell-*
405 *find* routine is separated into two phases. In the first phase, one element that contains the input
406 edge is searched by the following steps:
407

- 408 (1) Get the stored element incident to v_1 and push it into a stack;
- 409 (2) If the stack is empty, exit the routine and return NULL; otherwise, remove the top

- 410 element from the stack and go to Step 3;
411 (3) If the top element contains v_2 , return the top element and exit the routine;
412 (4) Flag the top element as *visited*, and then visit its neighboring elements. For any
413 unvisited neighbor, if it contains v_1 as well, push it into the stack;
414 (5) Go back to Step 2.

415 If no valid element is returned by the above procedure, the shell is empty; otherwise,
416 starting from the returned element, the entire shell can be visited by using the neighboring
417 indices of elements. In the worst scenarios, the first phase visits all elements surrounding v_1 ,
418 and the number of such elements is close to 30 on average for real mesh examples. The
419 second phase visits all elements surrounding the edge, and the number of such elements is
420 about 5-7 on average[‡]. Therefore, the first phase dominates a general calling of the routine in
421 terms of computing time. However, in many circumstances, one element surrounding an edge
422 is stored somewhere before calling the shell-find routine. By using this element as an extra
423 input, the timing-related performance of the shell-find routine can be improved remarkably by
424 skipping over the first phase.

425 5.3 Validity and optimality conditions.

426 The shell transformation routine presented in Algorithm 3 needs to output an *optimal*
427 covering mesh of a shell among all *valid* ones. Here, the definitions of validity and optimality
428 depend on specific application purposes. For mesh quality improvement, three types of
429 validation conditions are set for covering meshes as:

- 430 (1) *The basic condition*, which requires all elements have positive volumes.
431 (2) *The recursive condition*, which requires each shell transformation should create no
432 supporting faces around any *ancestor edge* of the current supporting edge.
433 (3) *The application specific condition*, in the context of mesh improvement, which requires
434 the quality of the output covering mesh of the shell should be higher than the quality of
435 the input covering mesh.

436 It is possible that more than one *valid* covering mesh exists for a shell. The final output of a
437 shell transformation calling is the covering mesh with the highest possible quality. See
438 Section 5.1 for the definition of *mesh quality*.

439 5.4 The shell transformation based local reconnection scheme

440 If one edge or face of a low-quality element is removed, the element will be removed
441 accordingly. Based on this concept, Algorithm 5 presents a local reconnection scheme that
442 attempts to remove low-quality elements by removing the edges or faces of these elements.

443 All of low-quality elements are stored in a heap in an ascending order of the element
444 quality. Firstly, Algorithm 4 is called on an edge of the first element of the heap. If the
445 element is removed by Algorithm 4, Algorithm 4 succeeds; otherwise, Algorithm 4 is
446 repeated on another edge of the element until all edges of the element are attempted. To
447 protect the mesh boundary, the edges attempted for removal must be interior edges of the
448 mesh. Next, if Algorithm 4 fails to remove the element, we attempt to remove the faces of this
449 element individually. To protect the mesh boundary, the faces attempted for removal must be
450 interior faces of the mesh. The 2-3 flip shown in Figure 1a is the simplest local scheme for
451 face removal. However, a more effective alternative is *multi-face removal* (see Figure 1c).

[‡] It is worth noting that both numbers could vary case by case, depending on mesh topologies. Nevertheless, the meshes considered in this study are inputs for numerical simulations, where only a small percentage of elements are badly shaped. For different meshes of this type, it is observed that both numbers usually remain within the ranges we mentioned in the text. For instance, for the unimproved F16 and Bridge meshes to be presented in Section 7 for tests, the average numbers of elements surrounding interior mesh nodes are both 5.50. After mesh improvement, these two numbers are reduced to 5.21 and 5.20 respectively. The numbers of elements surrounding interior mesh edges are 26.05 and 26.21, respectively. After mesh improvement, these two numbers are reduced to 23.82 and 23.80 respectively.

452 Shewchuk [10] suggested an implementation of multi-face removal. In this study, we present
453 an alternative solution based on the proposed shell transformation routine (i.e., Algorithm 3).

454 Given an interior face f for removal, the proposed algorithm takes the following steps as:

- 455 (1) Find two tetrahedra sharing face f , and denote the apexes of the tetrahedra opposite to f
456 as a and b , respectively.
- 457 (2) Find all of the faces opposite to a and b . As shown in Figure 9a, these faces may form
458 several connected components.
- 459 (3) Select a component that includes the face (or faces) intersected by ab , as shown in
460 Figure 9b.
- 461 (4) Define the boundary of the selected component as a polygon. If a point (such as p_7 in
462 Figure 9c) is contained in the interior of the polygon, remove one face (such as the face
463 $p_1p_2p_7$ in Figure 9c) incident on this point from the component.
- 464 (5) Now we get a local mesh like the one shown in the left of Figure 1c. With this mesh as
465 the input, *the shell transformation routine* (i.e., Algorithm 3) is called to search for a
466 better covering mesh to fill in the shell region.

467 To avoid an infinite execution of the loop defined in Lines 2-16 of Algorithm 5, no matter
468 the element for removal is removed or not, this element must be removed from the heap
469 before the next iteration.

470 **Algorithm 5.** The combinational edge removal based on recursive shell transformation

localReconnection(M, l_{\max})

Inputs:

the mesh to be improved, denoted M

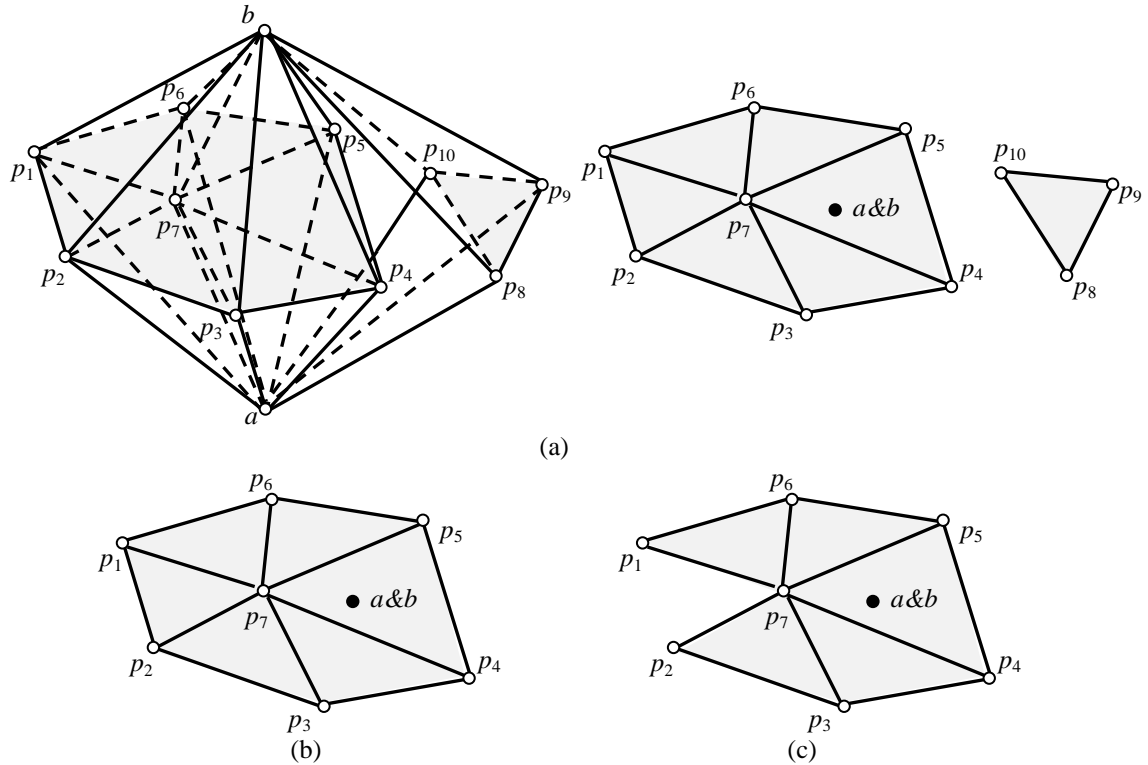
the maximally allowed recursive level, denoted l_{\max} and the default value is 5

Variables:

the heap that stores all of low-quality elements, T_{bad}

1. Insert all of low-quality elements into T_{bad} in the ascending order of the element quality
 2. **while** T_{bad} is not empty
 3. t : the first element of T_{bad}
 4. **If** t has been removed from M
 5. **goto** line 16
 6. $E = \{e_1, e_2, \dots, e_n\}$: the set of edges of t qualified for removal ($n \leq 6$)
 7. **for** $j = 1$ **to** n
 8. **recursiveST**($e_j, \emptyset, 0, l_{\max}$)
 9. **if** t is removed
 10. **goto** line 16
 11. $F = \{f_1, f_2, \dots, f_m\}$: the set of faces of t qualified for removal ($m \leq 4$)
 12. **for** $j = 1$ **to** m
 13. Remove f_j by a shell transformation based multi-face removal routine
 14. **if** t is removed
 15. **break**
 16. Remove t from T_{bad}
-

471
472



473
474

475
476
477

Figure 9. The procedure that prepares the inputs for the multi-face removal operation.

478

6. THE OVERALL MESH IMPROVEMENT ALGORITHM

479 The application goal of this study is to develop a cost-effective mesh improver. In this
480 section, we first present some basic considerations that guide this development procedure.
481 Then, we introduce the set of smoothing, point insertion and point suppression schemes
482 incorporated in our mesh improver. Finally, the overall mesh improvement scheme is detailed.

6.1. The basic considerations

484 In this study, the *minimum sine* of dihedral angles is used as a default quality measure. The
485 quality measure of a mesh is evaluated by a vector listing the quality of each tetrahedron
486 contained by the mesh, in an order from the worst to the best. Since the worst tetrahedron in a
487 mesh has far more influence than those average tetrahedra, the quality vectors of two meshes
488 are compared *lexicographically* so that, for instance, an improvement in the second-worst
489 tetrahedron improves the overall mesh quality even if the worst tetrahedron has not changed.

490 To ensure the heuristic algorithm never worsens the quality of a mesh, a *hill-climbing*
491 method is adopted in all of the developed local schemes, which considers applying a local
492 operation only if the quality of the changed mesh will be better than that of the original mesh.
493 Local operations that do not improve the mesh quality are not applied. The method stops
494 when no operation can achieve further improvement (i.e., the mesh is already locally optimal),
495 or when a further optimization promises too little gain.

496 Meanwhile, since the focus is usually on the worst tetrahedron, only *bad elements* are
497 treated to save the computing time, which refer to those elements whose minimum sine values
498 are less than 0.5 in the following discussions, i.e., at least one dihedral angle of the element is
499 either below 30° or above 150° .

500 The surface boundary of a volume mesh influences the mesh quality considerably. In the
501 applications where the boundary can be changed to some extents, it is beneficial to extend the
502 local schemes for mesh quality improvement from interior mesh entities to boundary entities.

503 However, in many applications, the improved mesh need to be consistent with a CAD model
 504 or matched face-to-face with another mesh. To limit the discussions, the presented algorithm
 505 regards the boundary configuration of the mesh as *untouchable*, i.e., vertices on the boundary
 506 cannot be smoothed, and the connectivity between them cannot be changed.

507 6.2. Smoothing

508 To achieve the cost-effectiveness, we combine an optimization-based algorithm [20] with the
 509 Laplacian smoothing to reposition each interior mesh point that is included by at least one bad
 510 element (referred to as a *bad point* hereafter):

511 (1) Perform Laplacian smoothing. If the improved *ball* (referring to all of elements incident
 512 on the point) contains no bad elements, the smoothing succeeds; otherwise, continue.

513 (2) Perform the optimization-based smoothing.

514 To save the smoothing time, a mesh point is flagged as *smoothed* after a successful
 515 smoothing, and this flag is flushed only if the ball of the point is changed. In each smoothing
 516 cycle, all of *non-smoothed bad* points are treated only once.

517 In each smoothing pass, the smoothing cycle is repeated until three indicators of the mesh
 518 quality are not improved further: (1) the quality of the worst tetrahedral (q_{worst}); (2) the
 519 number of bad elements (n_{bad}); and (3) the average quality of bad elements (q_{aver}).

520 6.3. Point insertion and point suppression

521 We adopt an *edge-splitting* based point insertion scheme. It attempts to insert a point at the
 522 middle of an interior edge and then to split those elements that meet at this edge; see Figure
 523 10a. Finally, the new point is smoothed, and if the resulting mesh is better than the old one,
 524 the mesh will be changed; otherwise, the old mesh is restored.

525 Besides, our mesh improver relies on an *edge contraction* operation to remove *bad* points
 526 of the mesh. Figure 10b illustrates this operation using a 2D example. Each edge ended with
 527 the point to be suppressed is contracted to the other endpoint, and the resulting mesh
 528 configuration with the best quality is selected for further smoothing. To save computing time,
 529 only the point that replaces the contracted edge is smoothed. The point suppression operation
 530 fails if edge contraction (plus point smoothing) cannot produce a better mesh than the old one.

531 Since only bad elements are targeted, those edges included by bad elements are attempted
 532 only once in each point suppression or insertion pass.

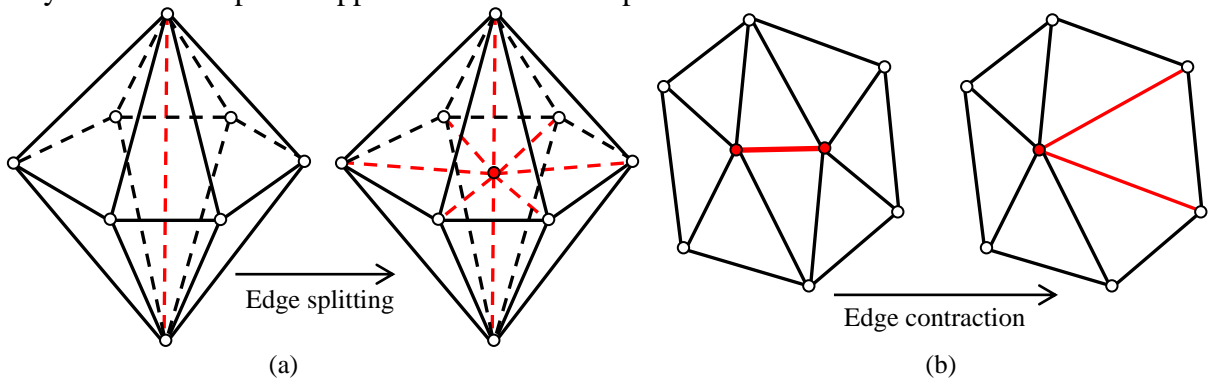


Figure 10. Illustration for the (a) edge splitting and (b) edge contraction operations.

536 6.4. The mesh improvement schedule

537 Algorithm 6 presents the proposed mesh improvement schedule, which combines different
 538 local schemes to improve the mesh quality. This schedule begins with a smoothing pass, and
 539 then executes the main loop of mesh improvement. In the main loop, a smoothing pass is
 540 followed after the pass of each type of topological transformations to improve the mesh
 541 quality further. The main loop is ended when three subsequent combinational passes fail to
 542 make sufficient progress or the number of iteration steps exceeds a predefined threshold (in

543 the present study, the default value of this threshold is 30). We gauge progress using three
 544 quality indicators mentioned in Section 5.4, i.e., q_{worst} , n_{bad} and q_{aver} .

545 **Algorithm 6.** The proposed mesh improvement schedule

improveAMesh(M)

Input:

M , the mesh to be improved

Variables:

q_{worst} , q'_{worst} , the quality of the worst tetrahedral

n_{bad} , n'_{bad} , the number of bad elements

q_{aver} , q'_{aver} , the average quality of bad elements

1. $failed = 0$; $itcount = 0$
 2. Smooth M
 3. Query the mesh quality and store the indicators in q_{worst} , n_{bad} and q_{aver} , respectively
 4. **while** $failed < 3$ && $++itcount \leq 30$
 5. **localReconnection**(M , 5)
 6. Smooth M
 7. Improve M by the point suppression scheme
 8. Smooth M
 9. Improve M by the point insertion scheme
 10. Smooth M
 11. Query the mesh quality and store the indicators in q'_{worst} , n'_{bad} and q'_{aver} , respectively
 12. **if** ($q'_{\text{worst}} < q_{\text{worst}} \parallel n'_{\text{bad}} < n_{\text{bad}} \parallel q'_{\text{aver}} < q_{\text{aver}}$) $failed = failed + 1$
 13. **else** $failed = 0$
 14. $q_{\text{worst}} = q'_{\text{worst}}$; $n_{\text{bad}} = n'_{\text{bad}}$; $q_{\text{aver}} = q'_{\text{aver}}$
-

546

547

7. RESULTS

548 The numerical tests are conducted on a PC workstation (CPU: 3.5GHz, Memory: 24GB).
 549 Results obtained from the developed mesh improver are compared with those obtained by
 550 Grumpp (Version 0.3.4) and Stellar (Version 1.0), respectively. To our knowledge, Grumpp
 551 [20, 32] and Stellar [12, 13] are among the best open-source improvers for tetrahedral meshes.
 552 Although many common features exist between two codes, their differences are also evident
 553 due to different start points of their development. The goal of Grumpp is to improve the
 554 worst tetrahedra cost-effectively, while the goal of Stellar is to improve the worst tetrahedra
 555 aggressively with speed as a secondary consideration.

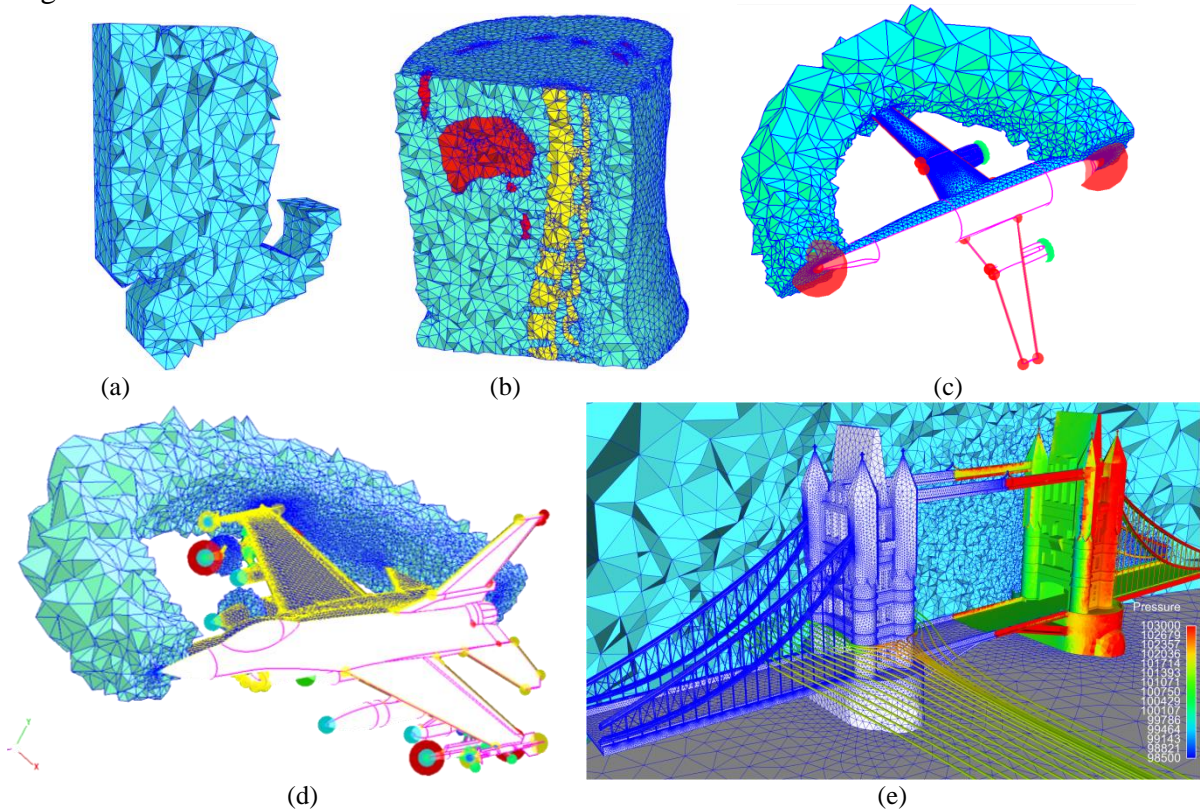
556 In default, Grumpp code takes four steps to improve a given mesh:

- 557 (1) Perform three passes of local reconnections for all elements.
- 558 (2) Perform two smoothing passes for elements containing angles below θ degrees or above
 559 $180 - \theta$ degrees. Here, θ is a threshold initially set as 25° and then adaptively reduced
 560 after each pass of smoothing operations.
- 561 (3) Repair a small fraction of the worst tetrahedra by a full range of swapping techniques.
- 562 (4) Repeat Step 2.

563 The default schedule of Stellar code begins with one smoothing pass, one local
 564 reconnection pass and one edge contraction pass for all elements, and then combines these
 565 local schemes and a point insertion scheme in a loop to improve the quality of a mesh
 566 iteratively. Inside this loop, the smoothing and local reconnection routines target at all

567 elements, but the most passes of edge contraction and point insertion routines target at
 568 elements with angles below 40° or above 140° except for a so-called *desperation pass*, which
 569 targets at the worst 3.5% of tetrahedra.

570
 571



572
 573

574 **Figure 11.** The selected meshes: (a) Tire; (b) Patient-organs02; (c) The F6 aircraft; (d) The
 575 F16 aircraft; (e) The London Tower bridge. Surface meshes and grid sources for mesh sizing
 576 control are displayed in both graph (c) and graph (d), and the surface mesh and inviscid flow
 577 simulation results induced by a crosswind are displayed in graph (e), respectively.

578 As shown in Figure 11, five meshes are selected. The first two meshes are accessible from
 579 the internet: the initial mesh of *tire* was ever analysed in literatures [20] and [32], and
 580 included in the package of Grumpp [32] and Stellar [13], and the initial mesh of *patient-*
 581 *organs02* is obtained from the AIM@SHAPE repository [33]. The last three meshes are
 582 generated by our in-house codes following the same schedule as:

- 583 (1) Input a geometry model.
- 584 (2) Triangulate the surface by an advancing front technique.
- 585 (3) Tetrahedralize the volume by a Delaunay mesher [4].

586 The original geometry models of the last three examples are all accessible from the internet.
 587 The London Tower Bridge model (referred to as *bridge* hereafter) and the DLR-F6 wing-
 588 body-nacelle-pylon aircraft model (referred to as *F6* hereafter) are the selected test case
 589 geometries for the meshing contest session of the 23rd International Meshing Roundtable
 590 (IMR) and the 2nd AIAA CFD Drag Prediction Workshop, respectively. The F16 aircraft
 591 model (referred to as *F16* hereafter) is obtained from GrabCAD [34].

592 Table 1 lists the initial mesh size statistics and the mesh quality data of those selected
 593 examples, where θ_{\min} and θ_{\max} refer to the minimum and maximum dihedral angles, and λ
 594 refers to the percentage of bad dihedral angles, i.e., angles within the range of $[0, 30^\circ]$ or
 595 $[150^\circ, 180^\circ]$, respectively. Meanwhile, λ_i ($i=1-5$) is used to evaluate the distributions of bad
 596 angles, which refers to the percentage of dihedral angles within the range of $[6(i-1), 6i]$ or
 597 $[180-6i, 180-6(i-1)]$ degrees. For instance, λ_2 refers to the percentage of dihedral angles within
 598 the range of 6° to 12° or 168° to 174° .

Table 1. The initial mesh size statistics and mesh quality data.

Examples	#tetra.	#points	θ_{\min} ($^{\circ}$)	θ_{\max} ($^{\circ}$)	% of bad angles (λ)	Distribution of bad angles (%)				
						λ_1	λ_2	λ_3	λ_4	λ_5
Tire	11,098	2,570	0.66	178.88	4.58	0.12	0.46	0.77	1.28	1.96
Patient-organs02	280,911	51,124	2.89	175.23	7.65	0.0072	0.21	1.20	2.45	3.78
F6	1,023,532	172,664	2.6e-13	≈ 180	6.65	0.23	0.68	1.19	1.82	2.73
F16	18,065,336	2,906,056	2.6e-14	≈ 180	6.63	0.23	0.67	1.18	1.82	2.74
Bridge	37,772,656	6,205,571	2.1e-13	≈ 180	6.72	0.23	0.68	1.19	1.85	2.77

600 In the first test, the performance data of different local reconnection schemes are compared
601 with each other. Stellar code executes edge removal and multi-face removal routines
602 repeatedly to improve mesh topology, while Grummp code executes 2-3 flips and edge
603 removal routines repeatedly. We improve the five initial meshes by performing one pass of
604 the three local reconnection schemes, respectively. Instead of improving all elements, only
605 *bad* elements are treated in this test. Table 2 presents the mesh quality and the computing time
606 data comparison.

607 For *patient-organs02*, *F6* and *F16* cases, our scheme not only achieves the lowest
608 percentage of bad angles (λ), but also narrows the ranges of dihedral angles to the largest
609 extent. For *bridge* case, our scheme also achieves the lowest λ ; however, all of the three local
610 reconnection schemes fail to improve both the smallest and the largest angles to an acceptable
611 level, although the values achieved by our scheme are slightly better. For *tire* case, Grummp
612 code improves θ_{\min} and θ_{\max} at the same level as our scheme. Meanwhile, Grummp code
613 achieves a slightly better value of λ than our scheme, while our scheme achieves smaller
614 values of λ_1 and λ_2 . We believe that, for this mesh, more angles between 12° and 30° (or
615 between 150° and 168°) are generated when our scheme attempts to remove small angles
616 between 0° and 12° or large angles between 168° and 180° , because the cost of improving the
617 worst angle is possibly increased considerably due to the generation of more undesirable
618 small/large angles.

619 In this test, Stellar code achieves the best performance with respect to the computational
620 time, while Grummp code performs rather well for small meshes but very poor for big
621 meshes. For our scheme, one pass of the proposed local reconnection scheme consumes more
622 time than its counterpart in Stellar code, because of its recursive nature. Nevertheless, since
623 the proposed scheme produces a much better mesh, this marginally more time consumption is
624 acceptable.

Table 2. The mesh quality and computational time data for different local reconnection schemes.

Examples	#tetra.	θ_{\min} ($^{\circ}$)	θ_{\max} ($^{\circ}$)	λ	Distribution of bad angles (%)					Time (s)	
					λ_1	λ_2	λ_3	λ_4	λ_5		
Tire	Grummp	11,019	3.36	172.38	4.21	0.069	0.30	0.57	1.18	2.09	0.09
	Stellar	10,936	3.00	172.38	4.23	0.056	0.31	0.59	1.23	2.05	0.07
	Present	10,906	3.36	172.38	4.42	0.047	0.27	0.61	1.30	2.19	0.21
Patient-organs02	Grummp	265,086	5.68	165.38	3.46	6.3e-5	3.3e-3	0.12	0.96	2.37	2.6
	Stellar	261,485	6.55	167.70	2.98	0	2.4e-3	0.089	0.79	2.09	2.6
	Present	259,959	11.21	162.59	2.81	0	6.4e-5	0.034	0.67	2.10	5.9
F6	Grummp	955,584	0.78	178.4	0.75	3.0e-4	2.0e-3	0.016	0.10	0.63	9.8
	Stellar	951,623	0.73	178.7	0.58	3.7e-4	4.3e-3	0.022	0.094	0.46	4.6
	Present	946,534	3.69	174.85	0.31	7.0e-5	4.8e-4	2.5e-3	0.018	0.29	5.7
F16	Grummp	16,854,123	2.4e-4	≈ 180	0.74	3.9e-4	2.3e-3	0.018	0.11	0.61	258.0
	Stellar	16,791,528	1.3e-4	≈ 180	0.57	9.5e-4	4.7e-3	0.024	0.097	0.45	72.6
	Present	16,682,773	3.80	174.20	0.31	1.9e-5	4.1e-4	4.1e-3	0.025	0.28	85.3
Bridge	Grummp	35,233,789	3.0e-5	≈ 180	0.81	2.5e-4	2.0e-3	0.017	0.11	0.67	542
	Stellar	35,081,252	9.2e-5	≈ 180	0.62	4.0e-4	3.8e-4	0.022	0.10	0.50	160.8
	Present	34,853,521	8.6e-4	≈ 180	0.36	1.5e-5	1.6e-4	1.9e-3	0.025	0.33	192.2

627 In the second test, we compare the default schedules of Grummp code, Stellar code and the

628 proposed algorithm (i.e., Algorithm 6). In this test, the option that prohibits the change on the
629 mesh surface is enabled for both Grummp and Stellar codes. In addition, because the first pass
630 of edge contraction in Stellar code can coarsen the input mesh dramatically, this pass is thus
631 disabled in this test.

632 Table 3 presents the mesh quality and computational time data from the second test. In all
633 of the cases, Grummp code outputs the worst quality meshes. For *F16* and *bridge* cases, the
634 meshes output by Grummp code contain extremely small and/or large angles, while Stellar
635 code and our algorithm can improve them to an acceptable level for further numerical
636 simulations. We believe that the following facts might account for the relatively poor
637 performance of Grummp code. Firstly, Grummp code does not incorporate any point
638 suppression and point insertion schemes. In practice, these two schemes are useful for
639 eliminating extreme small and/or large angles of a mesh. Secondly, Grummp code only
640 executes a fixed number of passes of swapping and smoothing operations. In both Stellar code
641 and our algorithm, the adopted scheduling strategies that combine local mesh improvement
642 schemes are far more aggressive.

643 **Table 3.** The mesh quality and computational time data of the default schedules of Grummp,
644 Stellar and our improved method.

Examples		#tetra.	#points	θ_{\min} ($^{\circ}$)	θ_{\max} ($^{\circ}$)	λ	Distribution of bad angles (%)					Time (s)
							λ_1	λ_2	λ_3	λ_4	λ_5	
Tire	Grummp	11,039	2,570	13.67	158.55	1.7	0	0	0.030	0.21	1.47	0.5
	Stellar	10,973	2654	23.4	148.1	0.15	0	0	0	0.017	0.13	106
	Present	11,840	2,751	20.67	157.45	0.26	0	0	0	0.018	0.24	1.0
Patient -organs02	Grummp	264,954	51,124	8.93	160.40	2.91	0	1.3e-4	1.6e-3	0.06	2.85	21
	Stellar	227,775	46,237	31.7	141.58	0	0	0	0	0	0	3,220
	Present	266,631	52,392	20.52	149.93	8.3e-3	0	0	0	3.8e-4	7.9e-3	16
F6	Grummp	955,512	172,664	0.78	178.4	0.65	1.7e-4	3.0e-4	1.1e-3	3.5e-3	0.65	43
	Stellar	918,434	171,912	18.2	158.7	5.9e-3	0	0	0	4.7e-4	5.4e-3	1,193
	Present	935,608	172,167	10.64	159.79	0.017	0	5.3e-5	3.2e-4	1.4e-3	0.015	26
F16	Grummp	16,854,105	2,906,056	2.4e-4	179.99	0.63	1.5e-4	3.2e-4	2.6e-3	0.010	0.62	884
	Stellar	16,360,678	2,910,076	3.8	174.2	0.027	6.1e-6	3.1e-6	1.1e-4	9.1e-4	0.026	9,882
	Present	16,666,517	2,923,840	3.8	174.2	0.013	6.0e-6	1.3e-5	7.7e-5	1.2e-3	0.012	522
Bridge	Grummp	35,233,695	6,205,571	3.0e-5	179.99	0.71	1.1e-4	2.0e-4	8.6e-4	6.8e-3	0.70	1,521
	Stellar	34,188,981	6,211,120	7.5	171.5	0.13	0	1.0e-4	4.2e-4	9.5e-4	0.13	21,779
	Present	33,698,234	6,091,180	5.79	172.55	0.13	9.9e-7	7.0e-5	4.0e-4	1.9e-3	0.13	1,412

645 In the second test, Stellar code outputs the best quality meshes in most occasions, and it not
646 only narrows the range of dihedral angles at most, but also reduces the percentage of bad
647 angles as well. For instance, for *patient-organs02*, Stellar code improves the smallest and the
648 largest angles to be 31.7° and 141.6° , respectively. In other words, the improved mesh does
649 not contain any bad angles. The mesh improved by our algorithm is slightly worse, which
650 contains 132 angles below 30° (of which 6 angles below 24°), but no angles above 150° . For
651 *F16* and *bridge* cases, the quality levels of the improved meshes by Stellar code and our
652 algorithm are very close.

653 With respect to the computational time performance, the proposed algorithm performs the
654 best in most cases, apart from the improvement of the mesh *tire*. For this smallest mesh,
655 Grummp code performs the best in terms of the timing performance. Here, we define a
656 *velocity* index to evaluate the timing performance as:

657 $v = \text{the number of elements contained in the input mesh} / \text{the total computing time.}$

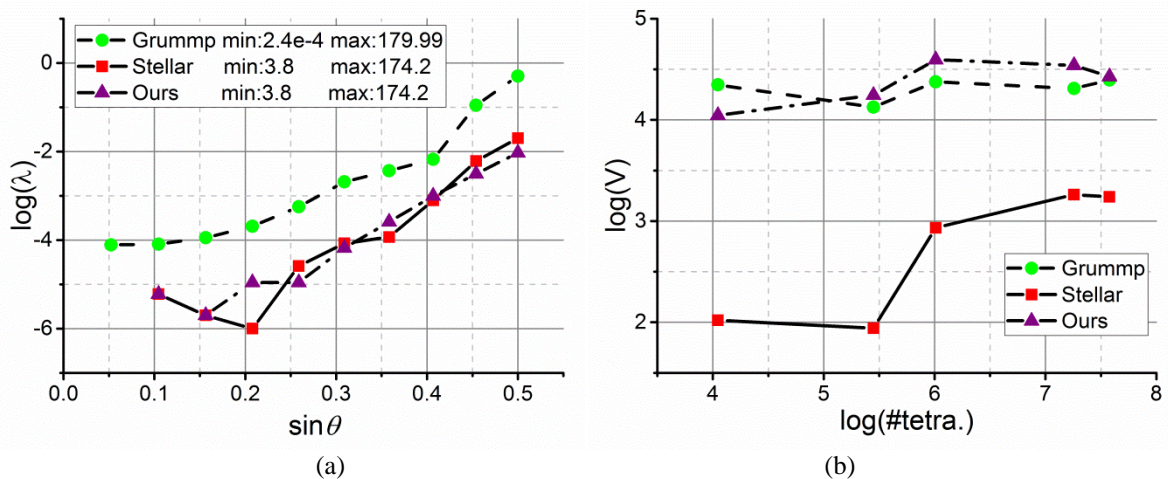
658 For those three inputs produced by the Delaunay mesher, i.e., *F6*, *F16* and *bridge*, Stellar
659 code runs at a speed of 45.9, 18.9 and 15.4 times slower than that of the proposed algorithm,
660 respectively. It is worth noting that the adopted Delaunay mesher runs very fast. For instance,
661 the generation of the initial mesh of *bridge* consumes only 174 seconds, while the proposed
662 algorithm can improve it to an acceptable mesh quality level for simulations in about 1,412
663 seconds. However, if replacing the proposed algorithm by Stellar code, it will take about 6

664 hours to achieve only marginal improvement (compared with our results) in terms of the mesh
 665 quality. In this respect, the proposed algorithm is undoubtedly a more *cost-effective* choice
 666 than the current default schedule of Stellar code.

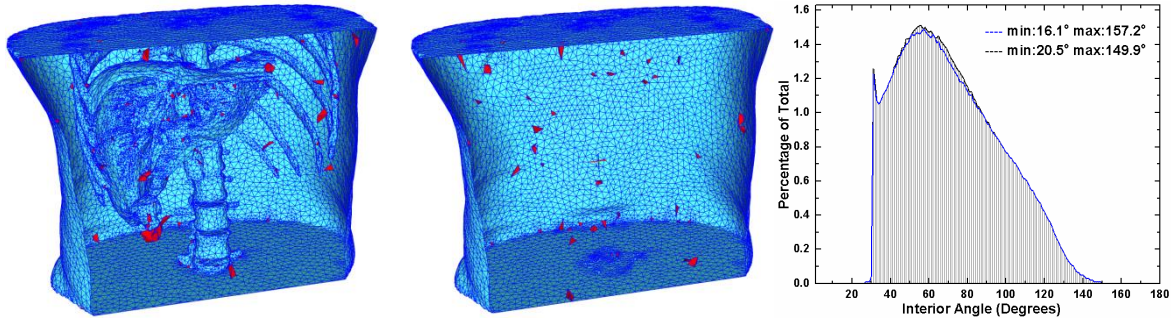
667 To demonstrate the performance difference between three mesh improvers more clearly,
 668 Figure 12a compares the distributions of bad angles of three F16 meshes produced by
 669 Grumpp code, Stellar code and our mesh improver. By default, each curve contains 10 data
 670 points, and the λ value of the i th point refers to the percentage of bad dihedral angles within
 671 the range of $[3(i-1), 3i)$ or $(180-3i, 180-3(i-1)]$ degrees ($i=1-10$). Nevertheless, because the
 672 meshes produced by Stellar code and our mesh improver contains no angles below 3° or
 673 above 177° , their corresponding curves contains no data points referring to angles within this
 674 range. Besides, Figure 12b compares the timing performance of three mesh improvers for five
 675 test meshes of various sizes, evaluated by the velocity indices of these improvers mentioned
 676 previously.

677 The λ value of each data point of the curve for Grumpp code is found larger than its
 678 counterparts from Stellar code and our mesh improver by nearly one or two orders of
 679 magnitude, while the λ values of data points of the curves for Stellar code and our mesh
 680 improver are comparable in general. However, the velocity indices of Stellar code are lower
 681 than their counterparts of Grumpp code and our mesh improver by one or two orders of
 682 magnitude, while the velocity indices of Grumpp code and our improver is at the same order.
 683 From the above analysis, we can conclude that our mesh improver presented in this study can
 684 achieve an overall better balanced performance between the mesh quality and computational
 685 time than other two state-of-the-art algorithms, and it is therefore more suitable for the quality
 686 improvement tasks involving large-scale meshes.

687 It needs to be pointed out that the initial mesh of *patient-organs02* actually contains interior
 688 constraints. However, because the current versions of Grumpp and Stellar codes provide no
 689 options to input a mesh with interior constraints, all of the tests presented above choose not to
 690 respect interior constraints. In fact, the proposed algorithm can respect interior constraints
 691 very well. To demonstrate this, Figure 13 compares the meshes improved by the proposed
 692 algorithm with or without interior constraints. Not surprisingly, the quality of the improved
 693 mesh that respects interior constraints is slightly worse.



694
 695
 696 **Figure 12.** A comparison of Grumpp, Stellar and our improver in terms of mesh quality and
 697 timing performance. (a) The distributions of bad angles of the F16 meshes produced by three
 698 improvers. (b) The velocity indices of three improvers for five test meshes.



699

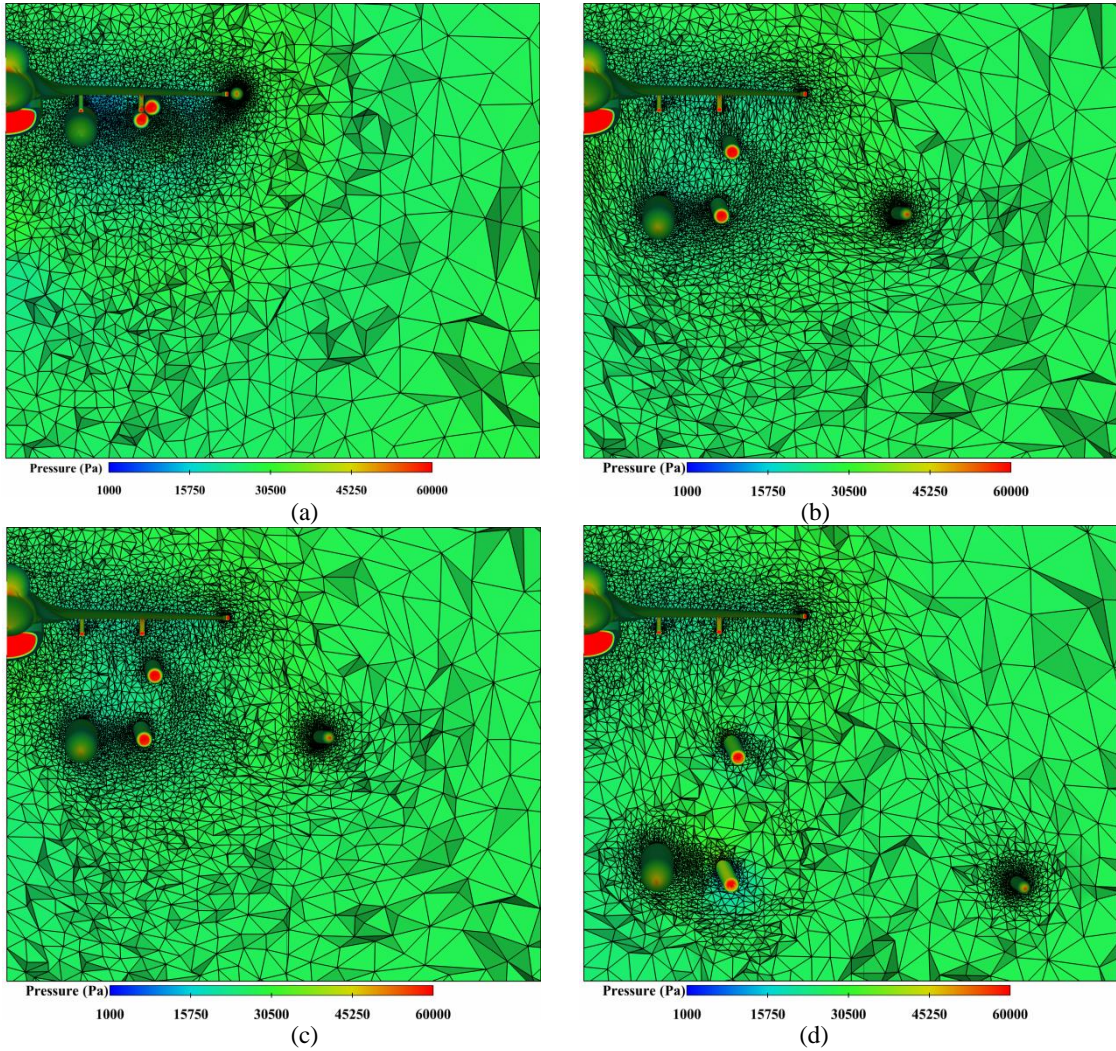
700 **Figure 13.** A comparison of the improved meshes of *patient-organs02* by the proposed
 701 algorithm with interior constraints respected or not. In graphs (a) and (b), the blue triangles
 702 are boundary triangles, and the red tetrahedra are elements containing dihedral angles below
 703 30° or above 150°. Graph (c) compares the distributions of dihedral angles of both meshes.

704 Finally, the applicability of the developed mesh improver for real aerodynamics
 705 simulations is demonstrated by a store separation simulation of a fully-loaded F16 aircraft. In
 706 this test, four stores are separated from the aircraft to verify the robustness of our in-house
 707 CFD system for complex flow simulations [35]. The main loop of this simulation includes
 708 four main steps:

- 709 (1) Compute the unsteady flow by a finite volume solver.
- 710 (2) Compute aerodynamic forces and moments based on flow simulation results, with
 711 which as inputs, the positions of moving bodies in the next time step are determined
 712 using the six degrees-of-freedom equations of motion.
- 713 (3) Move the mesh points to adapt the movement of mesh boundaries.
- 714 (4) If mesh movement yields elements with unacceptable quality, the holes are formed by
 715 deleting these elements. Next, a new mesh is formed by merging undeleted elements
 716 and new elements filled in the holes. Finally, the solution is reconstructed by
 717 interpolation.

718 The initial volume mesh is composed of about 3.69 million tetrahedral elements (see Figure
 719 14a). Figures 14b and 14c compare the meshes before and after local remeshing at $t_s = 0.147s$
 720 (t_s refers to a physical time of separation). Figures 14d presents the mesh at $t_s = 0.3s$, instantly
 721 after another local remeshing step is accomplished. Because the simulation involves very
 722 complicated boundary movements, the proposed remeshing algorithm is employed very
 723 frequently. Considering the simulation process until $t_s = 0.5s$, the remeshing algorithm is
 724 employed for a total of 44 times. On average, each local remeshing step needs to generate and
 725 improve a local mesh size composed of about 350K elements. Stellar code is obviously
 726 inappropriate for this kind of application because of its huge time consumption. Before this
 727 study, Grumpp code was ever employed for a local mesh improvement. It was observed that
 728 Grumpp code occasionally failed to provide a qualified mesh for simulations. One possible
 729 reason could be that mesh faces are largely stretched during the mesh deformation process
 730 and some of them may even appear on the boundaries of the holes to be remeshed. Grumpp
 731 code sometimes failed to remove those low-quality elements attaching to these stretched
 732 faces. After replacing Grumpp code with the present mesh improver, no failing case has been
 733 reported as far as this simulation is concerned.

734 Note that only the steps of the CFD solution and mesh deformation were executed in
 735 parallel on 32 computer cores in this test, while other steps, including local remeshing, are
 736 executed sequentially. Not surprisingly, the CFD solution step is most time-consuming, which
 737 used 91.9% of the total computing time. The mesh deformation step only used 3.9% of the
 738 total computing time because a simple spring-analogy approach was adopted [35]. Although
 739 local remeshing calling is executed sequentially, its total time cost is very low (using only
 740 2.9% of the total computing time).



741
742

743
744

745 **Figure 14** Cut views of the volume meshes for the store separation problem of a full-loaded
746 F16 aircraft at different physical time of separation (t_s): (a) $t_s=0s$; (b) $t_s=0.147s$, before local
747 remeshing; (c) $t_s=0.147s$, after local remeshing; (d) $t_s=0.3s$, after local remeshing.

748

8. CONCLUSIONS

749 A new flip named shell transformation is proposed for mesh quality improvement. Its single
750 calling could be considered as an enhanced version of the edge removal transformation, while
751 its recursive scheme acts like “composite edge removal transformations”. In practice, this
752 recursive scheme provides an elaborate pattern to combine multiple flips and perform these
753 flips on hundreds of elements for a single goal, for instance, removing a low-quality element
754 by removing one of its boundary edges. Accordingly, the possibility to achieve such a goal by
755 the proposed recursive scheme is much higher than those based on performing single flips
756 individually.

757 Furthermore, a new mesh improvement algorithm is developed by combining the proposed
758 local reconnection scheme with smoothing and other topological transformation schemes.
759 Numerical experiments have revealed that the proposed algorithm is capable of balancing the
760 requirements for a high-quality mesh and a low computational time costs spent on the mesh
761 improvement for large-scale engineering flow problems.

762

763 **Acknowledgements:** The authors appreciate the joint support for this project by the National Natural Science

764 Foundation of China (Grant No. 11172267, 11432013, 10872182) and Zhejiang Provincial Natural Science
765 Foundation (Grant No. LR16F020002 and Y1110038). The first author acknowledges the joint support from
766 Zhejiang University and China Scholarship Council and the host of Professor Oubay Hassan and Professor
767 Kenneth Morgan for his recent research visit to Swansea University, UK.

768
769 **REFERENCES**

- 770 [1] Weatherill NP, Hassan O. Efficient three-dimensional Delaunay triangulation with automatic point creation
771 and imposed boundary constraints. *Int. J. Numer. Methods Eng.* 1994; **37**:2005-2039.
- 772 [2] George PL, Borouchaki H, Saltel E. 'Ultimate' robustness in meshing an arbitrary polyhedron. *Int. J.*
773 *Numer. Methods Eng.* 2003; **58**:1061-1089.
- 774 [3] Du Q, Wang D. Constrained boundary recovery for three dimensional Delaunay triangulations. *Int. J.*
775 *Numer. Methods Eng.* 2004; **61**:1471-1500.
- 776 [4] Chen J, Zhao D, Huang Z, Zheng Y, Gao S. Three-dimensional constrained boundary recovery with an
777 enhanced Steiner point suppression procedure. *Comput. Struct.* 2011; **89**:455-466.
- 778 [5] Si H. TetGen, a Delaunay-based quality tetrahedral mesh generator. *ACM Trans. Math. Software* 2015;
779 **41**:11:1-11:36.
- 780 [6] Joe B. Construction of three-dimensional improved-quality triangulations using local transformations.
781 *SIAM J. Sci. Comput.* 1995; **16**:1292-1307.
- 782 [7] De L'Isle EB, George PL. Optimization of tetrahedral meshes. *IMA Vol. Math. Appl.* 1995; **75**:97-128.
- 783 [8] de Cougny HL, Shephard MS. Refinement, derefinement, and optimization of tetrahedral geometric
784 triangulations in three dimensions.1995. Unpublished manuscript.
- 785 [9] Misztal M, Bærentzen J, Anton F, Erleben K. Tetrahedral mesh improvement using multi-face
786 retriangulation. *Proceedings of the 18th International Meshing Roundtable*, Salt Lake City, UT, USA,
787 2009; 539-555.
- 788 [10] Shewchuk JR. Two discrete optimization algorithms for the topological improvement of tetrahedral
789 meshes. 2002. Unpublished manuscript. April-15-2016. URL: [https://www.cs.berkeley.edu/~jrs/papers/
790 edge.pdf](https://www.cs.berkeley.edu/~jrs/papers/edge.pdf).
- 791 [11] Klingner BM, Shewchuk JR. Aggressive tetrahedral mesh improvement. *Proceedings of the 16th*
792 *International Meshing Roundtable*, Seattle, WA, USA, 2007; 3-23.
- 793 [12] Klingner BM, Shewchuk JR. Stellar: a tetrahedral mesh improvement program. Jan-21-2016. URL:
794 <http://www.cs.berkeley.edu/~jrs/stellar>.
- 795 [13] Klincsek GT. Minimal triangulations of polygonal domains. *Ann. of Discrete Math.* 1980; **9**:121-123,
- 796 [14] Lo SH. 3D Delaunay triangulation of 1 billion points on a PC. *Finite Elem. Anal. Des.* 2015. **102-103**: 65-
797 73.
- 798 [15] Chen J, Zhao D, Huang Z, Zheng Y, Wang D. Improvements in the reliability and element quality of
799 parallel tetrahedral mesh generation. *Int. J. Numer. Methods Eng.* 2012; **92**:671-693.
- 800 [16] Zhao D, Chen J, Zheng Y, Huang Z, Zheng J. Fine-grained parallel algorithm for unstructured surface mesh
801 generation. *Comput. Struct.* 2015; **154**:177-191.
- 802 [17] Löhner R. Recent advances in parallel advancing front grid generation. *Arch. Computat. Methods Eng.*
803 2014; **21**:127-140
- 804 [18] Joe B. Construction of three-dimensional Delaunay triangulations using local transformations. *Comput.*
805 *Aided Geom. Des.* 1991; **8**:123-142.
- 806 [19] Compère G, Remacle JF, Jansson J, Hoffman J. A mesh adaptation framework for dealing with large
807 deforming meshes. *Int. J. Numer. Methods Eng.* 2010; **82**:843-867.
- 808 [20] Freitag LA, Ollivier-Gooch C. Tetrahedral mesh improvement using swapping and smoothing. *Int. J.*
809 *Numer. Methods Eng.* 1997; **40**:3979-4002.
- 810 [21] Liu J, Chen B, Sun S. Small polyhedron reconnection for mesh improvement and its implementation based
811 on advancing front technique. *Int. J. Numer. Methods Eng.* 2009; **79**:1004 -1018.
- 812 [22] Field DA. Laplacian smoothing and Delaunay triangulations. *Commun. Appl. Numer. Methods* 1988;
813 **4**:709-712.
- 814 [23] Freitag LA, Knupp PM. Tetrahedral mesh improvement via optimization of the element condition number.
815 *Int. J. Numer. Methods Eng.* 2002; **53**:1377-1391.
- 816 [24] Jiao X, Wang D, Zha H. Simple and effective variational optimization of surface and volume triangulations.
817 *Eng. Comput.* 2011; **27**:81-94.
- 818 [25] Leng J, Zhang Y, Xu G. A novel geometric flow approach for quality improvement of multi-component
819 tetrahedral meshes. *Comput.-Aided Des.* 2013; **45**:1182-1197.
- 820 [26] Vartziotis D, Wipper J. Fast smoothing of mixed volume meshes based on the effective geometric element
821 transformation method. *Comput. Methods Appl. Mech. Eng.* 2012; **201-204**:65-81.
- 822 [27] Vartziotis D, Wipper J, Papadrakakis M. Improving mesh quality and finite element solution accuracy by

- 823 GETMe smoothing in solving the Poisson equation. *Finite Elem. Anal. Des.* 2013. **66**: 36-52.
- 824 [28] Freitag DL, Knupp P, Munson T, Shontz S. A comparison of two optimization methods for mesh quality
825 improvement. *Eng. Comput.* 2006; **22**:61-74.
- 826 [29] Cheng S-W, Dey TK, Shewchuk JR. *Delaunay Mesh Generation*. CRC Press, Boca Raton, Florida,
827 December 2012.
- 828 [30] Bedregal C, Rivara MC. Longest-edge algorithms for size-optimal refinement of triangulations. *Comput.-*
829 *Aided Des.* 2014; **46**:246–251.
- 830 [31] Ruppert J, Seidel R. On the difficulty of triangulating three-dimensional non-convex polyhedra. *Discrete*
831 *Comput. Geom.* 1992; **7**:227-254.
- 832 [32] Ollivier-Gooch C. GRUMMP. April-15-2016. URL: <http://tetra.mech.ubc.ca/GRUMMP>.
- 833 [33] Model name: IRCADb_patient-organs02 (model ID: 1477-IRCADb_patient-organs02). April-15-2016.
834 URL: http://visionair.ge.imati.cnr.it:8080/ontologies/shapes/view.jsp?id=1477-IRCADb_patient-organs02.
- 835 [34] Guimarães GF. F-16 Fighting Falcon. April-15-2016. URL: [https://grabcad.com/library/f-16-fighting-](https://grabcad.com/library/f-16-fighting-falcon)
836 [falcon](https://grabcad.com/library/f-16-fighting-falcon).
- 837 [35] Zheng J, Chen J, Zheng Y, Yao Y, Li S, Xiao Z. An improved local remeshing algorithm for moving
838 boundary simulations. *Eng. Appl. Comp. Fluid* 2016. **10**: 405-428.